An Improved 2D Method of Moments for the Capacitance Calculation of Round Conductors with Insulation Layers

Luo, Tianming; Niasar, Mohamad Ghaffarian; Vaessen, Peter

DOI
10.1109/TPWRD.2025.3554662

Publication date
2025

Document Version
Final published version

Published in
IEEE Transactions on Power Delivery

An Improved 2D Method of Moments for the Capacitance Calculation of Round Conductors With Insulation Layers

Tianming Luo, *Member, IEEE*, Mohamad Ghaffarian Niasar, *Member, IEEE*, and Peter Vaessen, *Member, IEEE*

***Abstract*—Capacitance plays a crucial role in high dv/dt situations, making the accurate estimation of parasitic capacitance essential. This paper introduces an improved method of moments (MoM) for calculating the capacitance of round conductors, with or without insulation layers. The proposed method combines MoM with an analytical solution based on Laplace's equation. Compared to the original MoM, the proposed method does not require consideration of polarization charges on the surface of the insulation layer, which reduces the matrix size. Additionally, the proposed method can provide asymptotic formulas for capacitance calculation. The proposed method is compared with the 2D finite-element method (FEM), MoM and measurements. The results demonstrate that the proposed method aligns well with both the FEM simulations and the actual measurements. The proposed method uses less than half the time to calculate the same cases compared to the original MoM.**

***Index Terms*—Capacitance, method of moments, analytical formula, cable, windings.**

NOMENCLATURE

α_{ink}	Unkown coefficient of basis functions f_{nk} for mirror conductors.
α_{nk}	Unkown coefficient of basis functions f_{nk}.
ϵ	Permittivity.
$\Im$	Imaginary part of the value.
$\mathbf{C}$	Capacitance matrix.
$\mathbf{M}$	Moment Matrix.
$\mathbf{Q}$	Electric charge vector.
$\mathbf{V}$	Electric potential vector.
$\Re$	Real part of the value.
τ	Relation between A''_n and A'_n, B''_n and B'_n
A'_k, A''_k	Coefficients before the cosine terms in the general solution of Laplace's equation.
a_0	Radius of bare conductor.
a_t	Radius of the t^{th} insulation layer of conductor.
B'_k, B''_k	Coefficients before the sine terms in the general solution of Laplace's equation.
b_l	Half length of the line element l.
C	Capacitance.
C_0, D_0	Coefficients the constant term in the general solution of Laplace's equation.
E	Electric field.
f_{nk}	The k^{th} basis function of the conductor n.
I	Imaginary unit.
k	Order of the Fourier harmonic basis functions.
k_i	Image coefficient.
L	Number of line elements.
M	Number of conductors.
N	Maximal considered harmonic order.
Q	Electric charge.
Q_{i}	Mirror electric charge.
q_l	Electric charge distribution on the line element l.
q_n	Electric charge distribution on the conductor n.
r, φ	Coordinates in polar coordinates.
V	Electric potential.
V_0	Electric potential on a conductor.

Received 4 September 2024; revised 2 March 2025; accepted 23 March 2025. Date of publication 26 March 2025; date of current version 19 May 2025. This work was supported by Funding China Scholarship Council under Grant 202007720032. Paper no. TPWRD-01392-2024. *(Corresponding author: Tianming Luo.)*

Tianming Luo and Mohamad Ghaffarian Niasar are with the Department of Electrical Sustainable Energy, Delft University of Technology, 2628 CD Delft, The Netherlands (e-mail: t.luo-1@tudelft.nl; m.ghaffarianniasar@tudelft.nl).

Peter Vaessen is with the Department of Electrical Sustainable Energy, Delft University of Technology, 2628CD Delft, The Netherlands, and also with KEMA Laboratories, 6812DE Arnhem, The Netherlands (e-mail: p.t.m.vaessen@tudelft.nl).

Color versions of one or more figures in this article are available at https://doi.org/10.1109/TPWRD.2025.3554662.

Digital Object Identifier 10.1109/TPWRD.2025.3554662

I. INTRODUCTION

CAPACITANCE always plays an important role in high dv/dt situations due to its physical properties. In various components such as cables, transformers, and inductors, electromagnetic transient analysis is important to ensure reliable operation of power grids [1], [2], [3]. Transient response models can be classified as black, white, and grey-box models. Black-box models utilize measurements to determine the dynamic response and do not provide internal information [4]. The grey-box model is generally constructed based on lumped circuit elements, and the parameters are estimated with the help of the measurements [5]. The white-box models are based on physical laws and geometric information, which is helpful in understanding the transient response [6]. Capacitances are unavoidable and play a crucial role in transient analysis. Therefore, accurate capacitance estimation becomes a prerequisite for white-box models. Many methods have been developed to estimate capacitance.

In general, the capacitance calculation methods can be divided into two types: analytical methods and numerical methods. Two

methods are often used to obtain analytical models. One is based on energy conservation [7], [8], [9], which is often used for windings. It calculates the stored electric energy, equating it to the energy stored in an equivalent layer capacitance based on an assumed voltage distribution. However, it is difficult to apply this method to complex geometries. Another method is based on a capacitance network [10], [11], [12], [13], [14]. The capacitances in the network are calculated based on basic capacitance equations with an assumed electric field flux. The target capacitance is the equivalent capacitance of the formed network. The results can be different with different assumed field fluxes, as shown in [11]. Predicting field flux becomes challenging, especially with multiple conductors. The numerical methods are more versatile and can handle complex geometry. The common numerical methods include FEM [15], MoM [16], [17], charge simulation method [18] and finite difference method [19]. The FEM is based on approximating the solution in elements from the divided domain of interest. Compared to FEM, the MoM only needs a discretization of the boundary instead of the whole domain, which significantly reduces the matrix size. In [16], [20], MoM with Fourier harmonic basis functions has been used to calculate the capacitance per unit length of cables composed of round conductors with insulation. However, polarization charges on the insulation surface were introduced to meet the boundary condition, effectively doubling the matrix size.

This paper proposed an improved MoM, which uses the analytical solution to consider the insulation layer instead of using polarization charges. It does not introduce polarization charges and reduces the final matrix size. This results in a shorter computation time than the original MoM. The code for our proposed 2D method is available and shared at [21]. The paper is structured as follows. Section II introduces the theory of the proposed method. Section III introduces the choice of settings in the proposed method, the approximate capacitance equations and comparisons between the proposed method, 2D FEM, 2D MoM and measurements for specific configurations.

II. Theory of the Proposed Method

For a multi-conductor system, the voltage on one conductor is decided by the weighted sum of charges on all conductors. The weights form a symmetric matrix called the reciprocal capacitance matrix, which provides the relation between potentials and charges on conductors. Its inverse matrix is called capacitance matrix $\mathbf{C}$, which is used more often, and is shown in (1). Since the proposed method is a 2D method, values in $\mathbf{C}$ represent capacitance per unit length.

$$\mathbf{Q} = \mathbf{C}\mathbf{V} \tag{1}$$

This section first introduces the basic formulas of MoM. Next, the coupling of MoM and the analytical solution is introduced, which avoids introducing polarization charges. Then, the ground plane is dealt with the method of images and line element MoM.

A. Basic Formulas of MoM

The theory of MoM can be found in [20], [22]. This subsection briefly introduces the basic formulas used in round conductors.

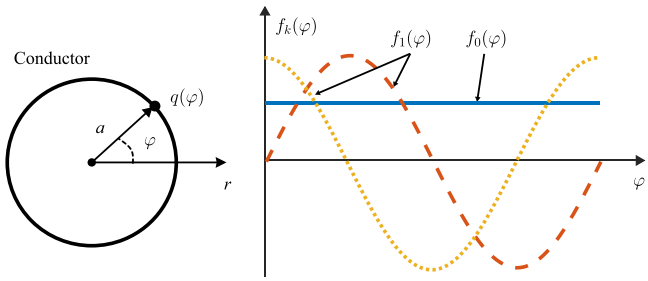

Fig. 1. Illustration of describing charge distribution with Fourier harmonics.

The MoM describes the charge distribution on the conductors' surface as the summation of a series of basis functions, as given in (2). The $q_n(l_n)$ is the charge distribution on the n^{th} conductor, l_n is coordinate function of the boundary. The α_{nk} is an unkown constant coefficient, f_{nk} is a known basis function, and k denotes the k^{th} basis function.

$$q_n(l_n) = \sum_{k=1} \alpha_{nk} f_{nk}(l_n) \tag{2}$$

For round conductors, the basis function often chooses Fourier harmonic functions (3), as shown in Fig. 1. N is the maximal considered harmonics. Including the constant term, a round conductor has $2N+1$ basis functions to describe the charge distribution. Since each harmonic has sine and cosine, the constant coefficients for sine and cosine are denoted by α_{snk} and α_{cnk}, respectively.

$$f_{nk}(\varphi_n) = \begin{cases} 1 & k = 0 \\ \cos(k\varphi_n) & k = 1 \ldots N \\ \sin(k\varphi_n) & k = 1 \ldots N \end{cases} \tag{3}$$

The potentials generated by charges following these basis functions can be obtained with the help of Green's function (4), where r is the distance from the charge to the tested point.

$$V = -\frac{1}{2\pi\epsilon} \ln r \tag{4}$$

The potentials generated by Fourier harmonic basis function are given in (5), where a_n is the radius of the n^{th} conductor and r_n is the distance from the centre of the n^{th} conductor to the point.

basis function	$V_{nk}(f_{nk})$
1	$-\frac{a_n}{\epsilon} \ln r_n$
$\cos(k\varphi_n)$	$\frac{a_n^{k+1}}{2\epsilon k r_n^k} \cos(k\varphi_n)$
$\sin(k\varphi_n)$	$\frac{a_n^{k+1}}{2\epsilon k r_n^k} \sin(k\varphi_n)$

(5)

Similar to the charge distribution, the potential can also described by Fourier harmonics, where all coefficients are zeros except the constant coefficient. Then, the equations describing the multiple round conductor systems can be built, like (6). The size of the matrix is $(2N+1)M \times (2N+1)M$, where M is

the number of round conductors.

$$\mathbf{V} = \mathbf{M}\mathbf{q} \tag{6}$$

The $\mathbf{V}$ is a vector of the potential on each conductor, which has the form

$$\mathbf{V} = [\mathbf{V}_1 \dots \mathbf{V}_n \dots]^T \tag{7}$$

where T denotes transpose. Each sub-vector in (7) is

$$\mathbf{V}_n = [V_n \;\; 0 \dots 0] \tag{8}$$

where V_n is the potential on the n^{th} conductor, zero terms are the coefficients of Fourier harmonics.

The $\mathbf{q}$ is a vector of the charge distribution on each conductor, which has the form in (9).

$$\mathbf{q} = [\mathbf{q}_1 \dots \mathbf{q}_n \dots]^T \tag{9}$$

Each sub-vector in (9) is a vector of unknown constant coefficients in (2) on a conductor.

$$\mathbf{q}_n = [\alpha_{n0} \dots \alpha_{nk}] \tag{10}$$

The $\mathbf{M}$ is a matrix describing the contribution from each charge distribution harmonic to each potential harmonic, which is derived from (5). The details are given in the appendix.

These are the basic equations of MoM when there are only bare round conductors. The charge distributions can be calculated by solving (6).

B. Coupling of MoM and Analytical Solution

The insulation layer of wires is considered by introducing polarization charges into (6) [16], [20], [22]. It doubles the size of matrix $\mathbf{M}$ when all conductors have an insulation layer. If conductors have multiple layers of insulation, the size of the matrix becomes even larger. The size of the matrix directly relates to the computation time for solving. By coupling MoM and analytical solution, introducing polarization charge can be avoided, reducing the time for solving equations. The analysis is based on two assumptions. One is that insulation layers are homogenous media. Then, the insulation layers are assumed to be concentric with the round conductors.

The background medium and insulation layers can be described by Laplace's equation. The general solution of the Laplace equation in polar coordinates is given in (11). Due to the periodical condition $V(r,\varphi) = V(r,\varphi+2\pi)$ and properties of trigonometric functions, the factor k can only be a non-negative integer. The voltage general solution is also composed of Fourier series. C_0 and D_0 are the coefficients related to constant term; A'_k and A''_k are the coefficients for sine; B'_k and B''_k are the coefficients for cosine.

$$V(r,\varphi) = C_0 + D_0 \ln(r) + \sum_{k=1}^{+\infty} \begin{Bmatrix} r^k (A'_k \cos k\varphi + B'_k \sin k\varphi) \\ +r^{-k} (A''_k \cos k\varphi + B''_k \sin k\varphi) \end{Bmatrix} \tag{11}$$

The structure of conductors with insulation layers is shown in Fig. 2. On the boundary Γ between t^{th} and $t-1^{\text{th}}$ layer of media, the boundary conditions (12) need to be fulfilled, where

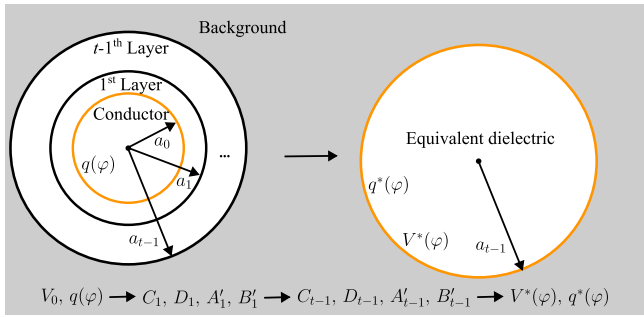

Fig. 2. Illustration of conductors with insulation layers and replacement with equivalent dielectrics.

q is the charges on the boundaries, subscript t denotes the t^{th} layer counting from inside to outside. When $t=0$, it represents the conductor.

$$\begin{aligned} \epsilon_t E_{rt}|_\Gamma - \epsilon_{t-1} E_{r(t-1)}|_\Gamma &= q|_\Gamma \\ E_{\varphi t}|_\Gamma &= E_{\varphi(t-1)}|_\Gamma \\ V_t|_\Gamma &= V_{t-1}|_\Gamma \end{aligned} \tag{12}$$

First, the boundary conditions on the boundary between the conductor and the medium around are analyzed. The relations in (13) are obtained. the free charge distribution and total charge amount are related to the solution of the Laplace equation in the dielectric.

$$\begin{aligned} D_1 &= -\frac{a_0}{\epsilon_1}\alpha_0 \\ A''_{k1}|B''_{k1} &= \tau_{1,0}(k) A'_{k1}|B'_{k1} \quad \tau_{1,0}(k) = -a_0^{2k} \\ A''_{k1}|B''_{k1} &= \xi_{1,0}(k) \quad \xi_{1,0}(k) = \frac{a_0^{k+1}}{2k\epsilon_1}\alpha_{ck}|\alpha_{sk} \\ C_1 + D_1 \ln(a_0) &= V_0 \end{aligned} \tag{13}$$

Then, the boundaries between dielectrics are analyzed, which can be between insulation layers or between the insulation layer and background medium. The space charge accumulated on the boundaries is ignored because space charge due to unmatched dielectric constant and conductivity between two dielectric does not have sufficient time to accumulate under AC stress. The relation in (14) is obtained from boundary conditions. The functions $\tau_{t,t-1}$ and $\xi_{t,t-1}(k)$ are given in (15).

$$\begin{aligned} A''_{kt}|B''_{kt} &= \tau_{t,t-1}(k) A'_{kt}|B'_{kt} \\ A''_{kt}|B''_{kt} &= \xi_{t,t-1}(k) \\ \epsilon_t D_t &= \epsilon_{t-1} D_{t-1} \\ C_t &= C_{t-1} + \left(1 - \frac{\epsilon_{t-1}}{\epsilon_t}\right) D_{t-1} \ln(a_{t-1}) \end{aligned} \tag{14}$$

$$\tau_{t,t-1}(k) = a_{t-1}^{2k} \frac{(\epsilon_t - \epsilon_{t-1}) a_{t-1}^{2k} + (\epsilon_t + \epsilon_{t-1}) \tau_{t-1,t-2}(k)}{(\epsilon_t + \epsilon_{t-1}) a_{t-1}^{2k} + (\epsilon_t - \epsilon_{t-1}) \tau_{t-1,t-2}(k)}$$

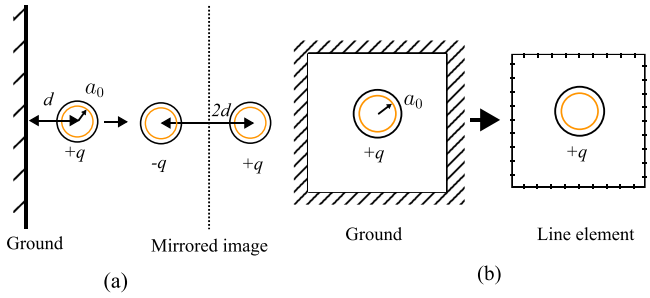

Fig. 3. Illustration of the method of image (a), line element (b).

$$\xi_{t,t-1}(k) = \left(\frac{\epsilon_t + \epsilon_{t-1}}{2\epsilon_t}\tau_{t-1,t-2}(k) + \frac{(\epsilon_t - \epsilon_{t-1})a_{t-1}^{2k}}{2\epsilon_t}\right) \times A'_{kt-1}|B'_{kt-1} \tag{15}$$

With the help of relations (13) and (14), the potential and charge distribution on the surface of the conductor are connected to boundary condition between the background medium and the most external insulation layer, i.e. the constant coefficients in (11) for $t-1^{th}$ layer. Then, an equivalent dielectric with radius a_{t-1} is generated. The equivalent charge distribution on the surface can be obtained through (13), as shown in Fig. 2. Based on the analysis in our previous work [23], the equivalent potential vector can be written as (16), which is related to the equivalent charge q^* through (14).

$$\mathbf{V}^* = [C_t + D_t \ln(a_{t-1}),\ \ a_{t-1}^k A'_{kt}, \ldots a_{t-1}^k B'_{kt}] \tag{16}$$

After applying MoM to the equivalent dielectric systems, the unknown virtual charge distribution and potential are solved. They are converted to the real potential and charge distribution through (13) and (14). During this procedure, no more polarization charges are introduced, and the size of the matrix remains the same.

C. Impact of Ground Planes

A plane and a rectangular tunnel are often used as the ground in various applications, playing an important role in the capacitance matrix. This subsection introduces two different methods for addressing the impact of ground planes. One is the method of images, and the other is the line element in MoM.

1) Method of Images: The method of images is a classic way to deal with ground planes in electrostatic [24]. As shown in Fig. 3(a), the boundary is replaced with a mirror charge Q_{i}, whose value is defined in (17). The coefficient k is the image coefficient and equal to -1 for the ground boundary.

$$Q_{\mathrm{i}} = k_{\mathrm{i}} Q \tag{17}$$

Based on the method of images, a matrix (6) involving both real and mirror conductors can be formed. However, when there is one ground boundary, it doubles the number of linear equations and slows down the calculation speed. It can be worse when multiple ground boundaries exist. Therefore, some manipulations are used to avoid adding more equations. After the mirror action, the charge distribution on the mirror image is described by (18), where subscript $_{\mathrm{i}}$ denotes the mirror conductor.

$$\begin{aligned} q_{\mathrm{i}} &= \alpha_{\mathrm{i}0} + \sum_{k=1} \alpha_{\mathrm{i}ck}\cos(k\varphi_{\mathrm{i}}) + \sum_{k=1} \alpha_{\mathrm{i}sk}\sin(k\varphi_{\mathrm{i}}) \\ &= -\alpha_0 - \sum_{k=1} \alpha_{ck}\cos(k(\pi-\varphi)) - \sum_{k=1} \alpha_{sk}\sin(k(\pi-\varphi)) \end{aligned} \tag{18}$$

The relations are obtained in (19). Based on these relationships, the equations introduced by the mirror conductors can be merged with those of the real conductors. The more equation equations due to the method of images are avoided.

$$\begin{aligned} \alpha_{\mathrm{i}0} &= -\alpha_0 \\ \alpha_{\mathrm{i}ck} &= -\alpha_{ck} \quad \text{k is even} \\ &\quad\ \alpha_{ck} \quad \text{k is odd} \\ \alpha_{\mathrm{i}sk} &= \alpha_{sk} \quad \text{k is even} \\ &\quad -\alpha_{sk} \quad \text{k is odd} \end{aligned} \tag{19}$$

2) Line Element in MoM: When the ground boundaries enclose the conductor, as shown in Fig. 3(b), applying the method of images often results in unbalanced mirror images or a non-zero net charge. It influences the accuracy of the calculation results. Therefore, the second method to deal with the ground plane is introduced as derived in [16].

It separates the ground boundaries and replaces them with line elements, as shown in Fig. 3(b), and form a matrix based on MoM. In this paper, constant elements are used. Each element is represented by a middle node on the element. One node means the elements have constant voltage and uniform charge distribution, i.e., the basis function only has a constant value α_0.

$$q_l(l_l) = \alpha_0 \tag{20}$$

The potential generated by the element can be calculated with Green's function, like (21).

$$V = -\frac{1}{2\pi\epsilon}\int_{l_n} q_l \ln(r - r^*)\mathrm{d}r^* \tag{21}$$

After introducing the line elements, the (6) become (22). The size of the matrix is $(2N+1)M + L \times (2N+1)M + L$, where L is the number of line elements.

$$\begin{bmatrix}\mathbf{V}_c \\ \mathbf{V}_l\end{bmatrix} = \begin{bmatrix}\mathbf{M}_{c\to c} & \mathbf{M}_{l\to c} \\ \mathbf{M}_{c\to l} & \mathbf{M}_{l\to l}\end{bmatrix}\begin{bmatrix}\mathbf{q}_c \\ \mathbf{q}_l\end{bmatrix} \tag{22}$$

The $\mathbf{V}_l$ is a vector of the potential on each line element, which has the form in (23), where each line element is one element in the vector.

$$\mathbf{V}_l = [V_1 \ldots V_l \ldots]^T \tag{23}$$

The $\mathbf{q}_l$ is a vector of the charge on each line element, which has the form in (24). Each line element has one element in the vector.

$$\mathbf{q}_l = [q_1 \ldots q_l \ldots]^T \tag{24}$$

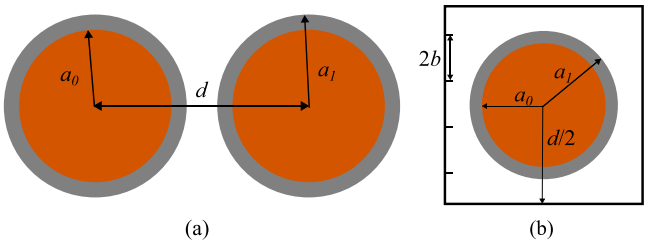

Fig. 4. Geometries used in setting choice, only round conductor (a), round conductor with a coaxial square box (b).

The details of $\mathbf{M}$ are given in the appendix.

III. Application of the Proposed Method

In this section, the capacitance C obtained from the proposed method, other analytical methods, FEM, MoM and measurements are compared under different situations. The FEM and MoM simulations use different physics interfaces of COMSOL software. Since the maximal harmonic order and the maximal length of line elements can vary in the proposed method and influence the results, a specific setting is needed for subsequent calculation. The first part determines the setting choice. Next, the proposed method is used to provide approximate analytical equations for capacitance between two parallel wires with or without an insulation layer. The results are compared with other analytical methods. After that, four different wire arrangements are computed by the proposed method, FEM and MoM, and measured with a vector network analyzer.

A. Setting Choice of the Proposed Method

For the proposed method, the choices of the maximal harmonic order N and the maximal line element length $2b$ influence the calculation results. Therefore, N and $2b$ need to be selected before the calculation. Two simple geometries are used, as shown in Fig. 4. Fig. 5(a) and (b) show the relative error compared to 2D FEM with geometry in Fig. 4(a), i.e., two parallel wires without and with insulation layer, respectively. With increasing N, the relative error decreases. For two bare wires, the error can be reduced to below 1% when $N = 2$ and $d/2a_0 > 1.25$. The same accuracy can be achieved when $N = 6$ and $d/2a_0 > 1.05$. For wires with insulation wires, the error increases with decreasing $d/2a_1$ and a_1/a_0. If the $a_1/a_0 = 1.1$, the error can be below 1%, when $N = 2$ and $d/2a_1 > 1.2$, or when $N = 6$ and $d/2a_1 > 1.02$.

Fig. 5(c) shows the relative error of capacitance between a coaxial square box and a wire with an insulation layer, Fig. 4(b). The calculation is performed by varying the ratio b/a_0 while keeping $N = 6$. With a smaller ratio, the number of line elements increases. The error does not exceed 5% in the calculated range when b/a_0 is $1/2$. With smaller b/a_0, the accuracy can be better, but the number of elements is larger, which leads to longer computation time. Therefore, b/a_0 is set to $1/2$.

After the comparison for a simple case, the configuration $N = 6$ and $b/a_0 = 1/2$ is chosen to ensure accuracy while maintaining a reasonable computational time for the case study.

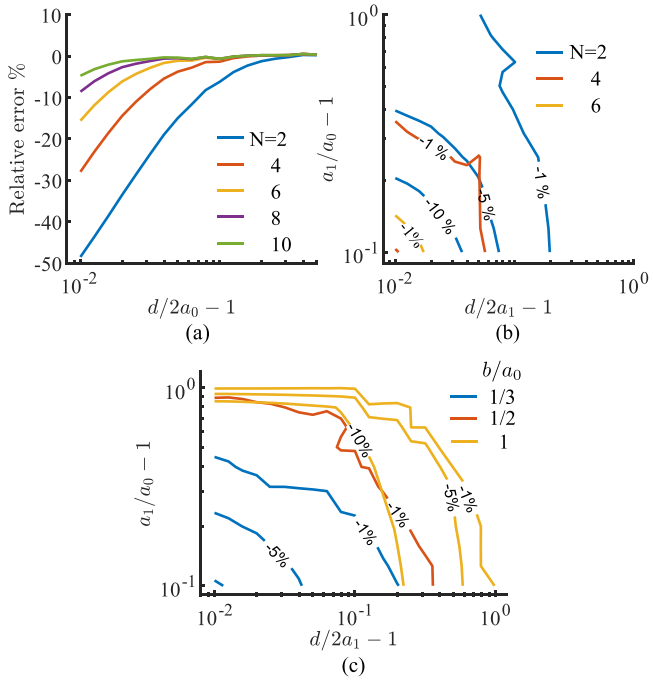

Fig. 5. Relative error of capacitance between two parallel wires with different maximal harmonic order N compared to 2D FEM, wires without insulation layer (a); wires with insulation layer (b); relative error of capacitance between coaxial square box and a wire with insulation layer and tunnel with different maximal size of line element b/a_0 (c). The number on the contour is the relative error in (b) and (c).

B. Approximate Analytical Formulas

The proposed method can be used to obtain approximate analytical capacitance formulas. Three capacitance formulas for two parallel wires under different situations are provided as examples. In general, considering higher-order harmonics N results in more accurate approximate formulas. However, this also leads to more complex formulas, which are not suitable to include in the paper. Therefore, in the paper, the order used depends on the complexity of the formulas that were obtained.

The first example is the capacitance between two bare conductors. It is similar to the one in Fig. 5(d), except that there is no insulation layer. The analytical formula is given in (25), where R_{da} is the ratio of distance d to radius a. When setting $N = 2$, the proposed method provides the approximate formula (26). The results are compared to 2D FEM, and the relative errors are shown in Fig. 6(a). The (26) is closer to (25) with increasing R_{da}, and the error is less than 1% when $d/2a > 1.25$.

$$C = \frac{\epsilon_0 \pi}{\operatorname{arcosh}(R_{da}/2)} \quad R_{da} = \frac{d}{a} \tag{25}$$

$$C = \frac{\epsilon_0 \pi}{\dfrac{3 - R_{da}^2 - 2R_{da}^4}{2 - 6R_{da}^2 - 2R_{da}^4 + 2R_{da}^6} + \ln\left(R_{da}\right)} \tag{26}$$

The second example is the capacitance between two parallel wires with an insulation layer, which is the same as the one in Fig. 5(d). A formula is given in (27) [25], where R_{db} is the ratio of the distance d to outer radius a_1, and R_{ba} is the

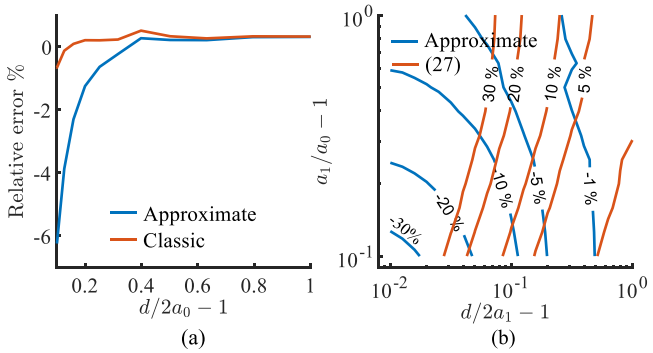

Fig. 6. Relative error of capacitance formulas compared to 2D FEM, two wires without insulation layer (a), two wires with insulation layer (b).

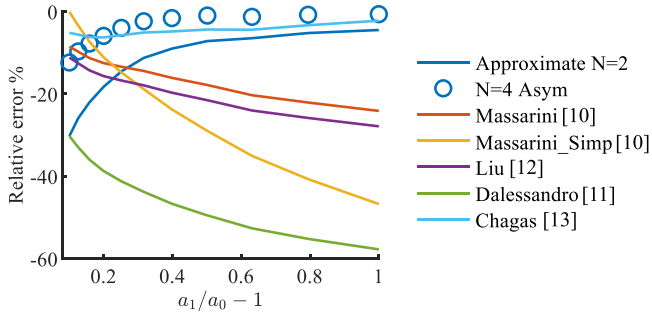

Fig. 7. Relative error of capacitance formulas for adjacent wires compared to 2D FEM.

ratio of the outer radius a_1 to the inner radius a_0. When setting $N = 1$, the proposed method can yield the approximate formula (28). Fig. 6(b) shows the relative error contour compared to 2D FEM. Formula (27) overestimates the capacitance, and the relative errors are sensitive to the value of R_{db}. The higher R_{db}, the relative errors are less. The approximate formula (28) underestimates the capacitance when both R_{db} and R_{ba} are small. According to the figure, (28) is more accurate than (27) in most cases. Formula (27) is obtained from a series combination of capacitance related to the insulation layer and the air gap, and the error is caused by the unmatched electric flux line.

$$C = \frac{\pi\epsilon_0}{\ln\left\{R_{ba}^{\epsilon_0/\epsilon_{\text{ins}}}\left[R_{db}/2 + \sqrt{(R_{db}/2)^2 - 1}\right]\right\}} \tag{27}$$

$$C = \pi\epsilon_{\text{ins}}\epsilon_0 \Big/ \Big\{\epsilon_{\text{ins}} \ln(R_{db}) + \epsilon_0 \ln(R_{ba}) + \frac{((1+R_{ba}^2)\epsilon_{\text{ins}} + (1-R_{ba}^2)\epsilon_0)\epsilon_{\text{ins}}}{((1+R_{ba}^2)(1-R_{db}^2)\epsilon_{\text{ins}} + (1-R_{ba}^2)(1+R_{db}^2)\epsilon_0)}\Big\} \tag{28}$$

The last example is the adjacent two wires with insulation wires. This situation attracts much attention because it is related to the turn-to-turn capacitance in windings. In [10], [11], [12], [13], the capacitances are calculated based on capacitance networks with different assumed electric flux lines. The approximate formula has the form (29), where $F(N)$ is a rational function of R_{ba} is larger than and ϵ_{ins}. In appendix 2, $F(2)$ and an asymptotic form of $F(4)$ are given.

$$C = \frac{\pi\epsilon_0}{\ln(2) + \ln(R_{ba})/\epsilon_{ins} - F(N)} \tag{29}$$

Fig. 7 shows the relative error compared to 2D FEM. For comparison, the integral form formulas from [10], [11], [12], [13] and the simplified formula from [10] are used. For the capacitance between two adjacent wires, the integration range is set from $-\pi/2$ to $\pi/2$, except that it has to be from $-\pi/6$ to $\pi/6$ in [11]. Among all formulas based on capacitance networks, [13] shows the most accurate results. The asymptotic form of the formula with $N = 4$ shows better accuracy than [13] when R_{ba} is larger than 1.25. The formula with $N = 2$ is less accurate than [13], but it shows comparable accuracy at high R_{ba}.

TABLE I
DETAILS OF GEOMETRIES OF 4 CASES

No.	case 1	case 2	case 3	case 4
Type	(a)	(c)	(b)	(d)
d [mm]	8.5	8.5	8.5	8.5
a_1 [mm]	4.25			
a_0 [mm]	2.65			
Δh [μm]	85			
wid [mm]	Not Applied		30	
hei [mm]	Not Applied		30	

Based on three examples, it is shown that the approximate formulas obtained from the proposed method have good accuracy, especially when wires have large distances and/or thick insulation layers.

C. Multiple Conductors with/without Enclosing Ground

In subsection A, the setting of the proposed method was chosen. In this subsection, the proposed method is verified on four multiple conductor cases, which have a plane ground or an enclosing ground. The capacitance in cases is simulated and measured on 1 m long wires. The measurements were done with the vector network analyzer Bode 100. The vector network analyzer used the series-thru configuration because of the high impedance of the samples. The capacitances were measured between 1 kHz to 1 MHz.

The insulation layer is made of PVC. Since the permittivity of the PVC varies with frequencies, the relative permittivity is measured. The relative permittivity in the frequency range of measurement is fitted by the formula (30).

$$\epsilon_r = 4.484 - 0.2477 \log_{10} f \tag{30}$$

The geometries of sample cases are shown in Fig. 8, and details are provided in Table I. Δh is the thickness of insulation tape used to fix the cable geometry. The harmonic order N is 6, and the length of element $2b$ is a_0. In cases 1 and 2, the wires are placed on the grounded plane. In cases 3 and 4, the wires are placed in a grounded tunnel and positioned along the centreline of the bottom. All cases consist of three wires, and the capacitance matrix C has the form given in (31). C_{aa}, C_{bb} and C_{cc} are the self-capacitance of each wire, which includes

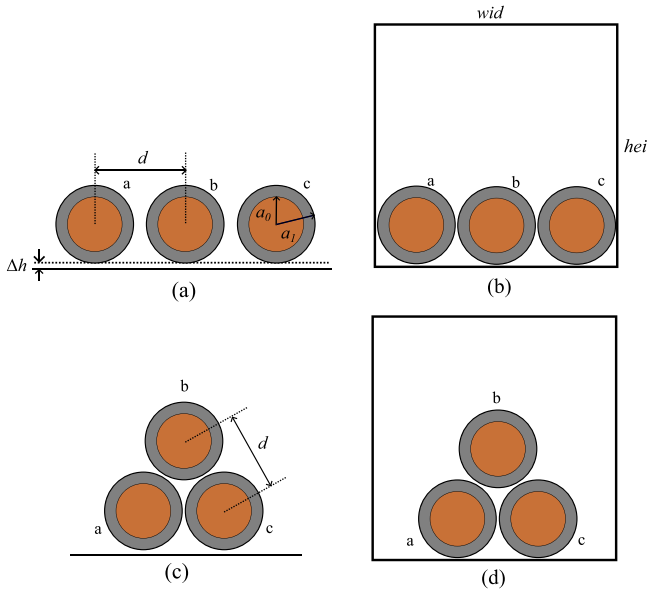

Fig. 8. Four geometries used in the simulations and measurements.

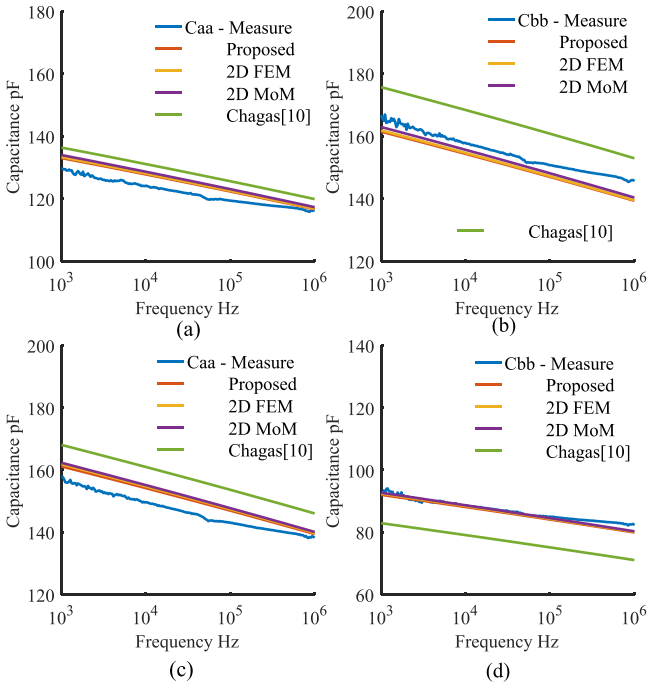

Fig. 9. Capacitance of 1 m wires from measurement, the proposed method, 2D FEM, 2D MoM and [13]. The (a) for C_{aa}, (b) for C_{bb} in case (1); (c) for C_{aa}, (d) for C_{bb} in case (2).

the capacitance between the wire and ground and the mutual capacitance between wires. The accuracy of calculations is verified by comparing the self-capacitance values. The capacitance is measured between one wire and the ground when two other wires are grounded. Three self-capacitances are obtained by applying the same process on three wires sequentially. Since the geometries are symmetric, all capacitances related to the side wires should be the same, for example, $C_{aa} = C_{cc}$.

$$\mathbf{C} = \begin{bmatrix} C_{aa} & -C_{ab} & -C_{ac} \\ -C_{ab} & C_{bb} & -C_{bc} \\ -C_{ac} & -C_{bc} & C_{cc} \end{bmatrix} \tag{31}$$

Except for measurements, the original Fourier series based MoM [16], [20], capacitance network based on [13] and FEM and MoM static electric field modules in COMSOL software are calculated for comparison. Using the method in [13] needs to set the integration limits first, which are determined based on the value used in [13]. If there is an air gap between wires or wire and ground, the capacitances are regarded as a series connection of the turn-turn capacitance and the air-gap capacitance.

Since the result of the original Fourier series based MoM are the same as those from the proposed method, the results are not show independently in Figs. 9 and 10. Fig. 9 shows the capacitance results of cases 1 and 2, which have a ground plane. The results from the proposed method, 2D FEM and 2D MoM, almost overlap in the cases. This implies that the proposed method can accurately calculate the theoretical capacitance of the geometries considered. In the frequency range of the measurement, the changes in measured capacitance follow the trend of the fitted relative permittivity curve. For case 1, as shown in Fig. 9(a), the measured C_{aa} is roughly higher than calculated results by 2 to 4%, the measured C_{bb} is lower than calculated results by up to 3%. For the results with [13], even if it considers the different integration limits, the difference between C_{aa} and C_{bb} is still larger than the measurements. It indicates that the summation of capacitance can lead to more errors in compact wire arrangements. For case 2, the differences between the proposed method and measurements are up to about 2%. Results from the capacitance network have a bit larger error, which is up to 10%. The relative error between measurement and calculation with the proposed method may result from variations in measured geometry. The errors of capacitance in case (1) and C_{aa} in case (2) are greater than the errors of C_{bb} in case (2). The reason can be attributed to the geometry variation being larger between a cable and ground plane compared to between cables. Cables are fixed by insulation tape and easily form a good alignment. C_{bb} in cases (2) are mainly contributed by the capacitance between cables since their trefoil shape. Therefore, the lower distance variation leads to smaller errors compared to other capacitance in cases (1) and (2).

Fig. 10 shows the results for cases 3 and 4. The similarities between the results from the proposed method, 2D FEM, and 2D MoM prove the effectiveness of the proposed method in dealing with the enclosing ground. Due to the similar wire structure, the capacitance C_{aa} and C_{bb} for cases 3 and 4 follow similar curves as in cases 1 and 2, except with higher values due to the enclosing ground. The relative error of the proposed method is up to 7% and is less than that of the capacitance network. The errors of C_{aa} in cases (3) and (4) are greater than that in cases (1) and (2). It may be caused by variations in the distance not only between the cable and the bottom wall of the grounded box, but also between the cable and the lateral wall,

Based on the comparison between results from measurements and used methods, the accuracy of the proposed method is

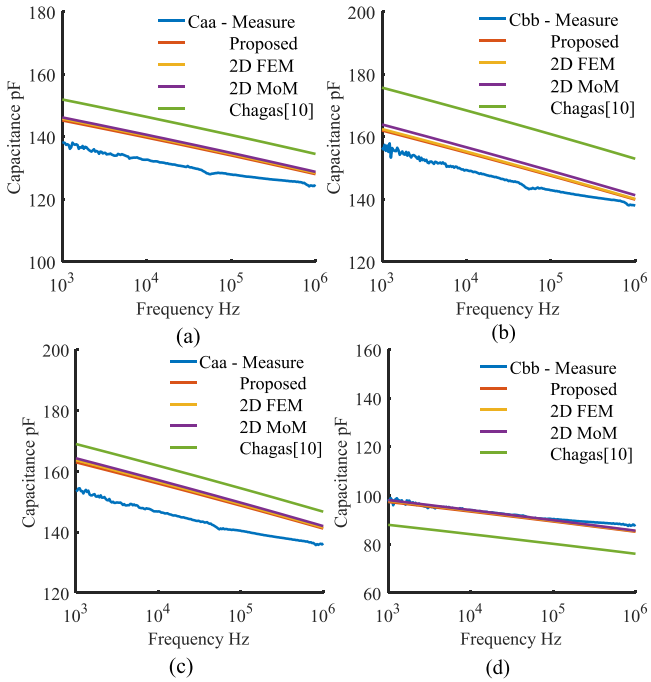

Fig. 10. Capacitance of 1 m wires from measurement, the proposed method, 2D FEM, 2D MoM and [13]. The (a) for C_{aa}, (b) for C_{bb} in case (3); (c) for C_{aa}, (d) for C_{bb} in case (4).

TABLE II
COMPUTATION TIME FOR 4 CASES

Method	Proposed	2D FEM	2D MoM	[13]	[16], [20]
Time(s)	1.40	177	137	4.63	3.53

validated. The smaller matrix size of the proposed is the main difference from the original MoM, which should lead to fast computational speed. The computational time for the cases is listed in Table II. Since the proposed method does not need polarization charge, the time used to construct relative matrix is saved and the time used to solve the matrix is reduced. The original MoM spends 3.53 s on calculation for 4 cases, which is more than double the time used for the proposed method. Besides, it is shown that the proposed method is two orders of magnitude faster than commercial software and faster than the capacitance network with integration.

IV. CONCLUSION

This paper introduces an improved MoM method for 2D capacitance calculation of round conductors with/without insulation layers. Through coupling the MoM and analytical solution, the conductors with insulation layers are able to convert to equivalent charge and potential boundary conditions on a circle, which avoids introducing polarization charge. It leads to half the matrix size compared to the original MoM. The proposed method is able to provide approximate capacitance formulas under different situations, which can have better accuracy than existing formulas in some geometry ranges. Then, the proposed method is validated for multiple conductor cases. Through comparing with the measurements, 2D FEM, 2D MoM and capacitance network. The results from the proposed method almost overlap with that of 2D FEM and 2D MoM and have up to 7% error compared to measurements. The computation time of the proposed method is two orders of magnitude faster than that of commercial software and is less than half of that with the used capacitance network.

APPENDIX

A. Detail of Matrix

In the appendix, the details of matrix $\mathbf{M}$ are given. The matrix can separated into four parts as shown in (22). Each part is composed of several submatrixes.

The submatrix in $\mathbf{M}_{c\to c}$ represents the contribution from the charges on conductors to the potentials on conductors. The contributions from the constant basis function term on conductor n to potential terms on conductor m are given in (32), where subscript j denotes the order of the potential harmonic, ranging from 1 to N. The first column is the basis function of the potential of the conductors. The (33) provides the formulas for the symbols used to simplify the (32), where subscript i denotes the order of the charge harmonic. x_{nm} and y_{nm} represent the distances between center of conductors in coordinates.

	Coefficents α_{n0}	
	$n \neq m$	$n = m$
1	$-\frac{a_n}{2\epsilon}\ln\left(x_{nm}^2+y_{nm}^2\right)$	$-\frac{a_n}{\epsilon}\ln(a_n)$
$\cos(j\varphi_m)$	$-\frac{a_n}{j\epsilon}\Re\left(\eta_{1j}\phi_{0j}\right)$	0
$\sin(j\varphi_m)$	$-\frac{a_n}{j\epsilon}\Im\left(\eta_{1j}\phi_{0j}\right)$	0

(32)

$$x_{nm}=x_m-x_n \qquad y_{nm}=y_m-y_n$$
$$\eta_{ij}=\frac{(i+j-1)!}{(i-1)!j!} \qquad \phi_{ij}=\frac{(-a_m)^j}{(x_{nm}-Iy_{nm})^{i+j}} \tag{33}$$

The contributions from the harmonic basis function term on conductor n to potential terms on conductor m are given in (34), when $n \neq m$. Otherwise, the contribution is zero.

	Coefficents α_{cni}	Coefficents α_{sni}
1	$\frac{a_n^{i+1}}{2i\epsilon}\Re\left(\eta_{i0}\phi_{i0}\right)$	$\frac{a_n^{i+1}}{2i\epsilon}\Im\left(\eta_{i0}\phi_{i0}\right)$
$\cos(j\varphi_m)$	$\frac{a_n^{i+1}}{2i\epsilon}\Re\left(\eta_{ij}\phi_{ij}\right)$	$\frac{a_n^{i+1}}{2i\epsilon}\Im\left(\eta_{ij}\phi_{ij}\right)$
$\sin(j\varphi_m)$	$-\frac{a_n^{i+1}}{2i\epsilon}\Re\left(I\eta_{ij}\phi_{ij}\right)$	$-\frac{a_n^{i+1}}{2i\epsilon}\Im\left(I\eta_{ij}\phi_{ij}\right)$

(34)

The submatrix in $\mathbf{M}_{c\to l}$ represents the contribution from the charges on conductors to the potentials on line elements. Since the potentials on the line elements only have constant basis function, the formulas are the same as the formulas for constant basis function in (32) and (34).

The submatrix in $\mathbf{M}_{l\to c}$ represents the contribution from the charges on line elements to the potentials on conductors. Formulas for two kinds of line elements are given in (A), where b_l is the half length of the element. One kind of element is parallel to the y-axis, and another is parallel to the x-axis. For other

direction line elements, some manipulations on trigonometric functions are needed. Some symbols in (36) are used to simplify the (A).

	Coefficents of elements along x-axis α_{l0}
1	$-\frac{1}{4\pi\epsilon}\Re\left(-4b_l+\mathcal{G}(x_{nm},y_{nm})\right)$
$\cos(\varphi_m)$	$-\frac{a_m}{4\pi\epsilon}\ln\left(\frac{((x_{nm}+b_l)^2+y_{nm}^2)}{((x_{nm}-b_l)^2+y_{nm}^2)}\right)$
$\sin(\varphi_m)$	$\frac{Ia_m}{4\pi\epsilon}G(x_{nm},y_{nm})$
$\cos(j\varphi_m)$ $j\geq 2$	$-\frac{a_m^j}{4j\pi\epsilon}\begin{pmatrix}T_1(x_{nm},y_{nm},j-1)\\+T_2(x_{nm},y_{nm},j-1)\end{pmatrix}$
$\sin(j\varphi_m)$ $j\geq 2$	$-\frac{Ia_m^j}{4j\pi\epsilon}\begin{pmatrix}T_1(x_{nm},y_{nm},j-1)\\-T_2(x_{nm},y_{nm},j-1)\end{pmatrix}$

(35)

	Coefficents of elements along y-axis α_{l0}
1	$-\frac{1}{4\pi\epsilon}\Re\left(-4b_l+\mathcal{G}(y_{nm},x_{nm})\right)$
$\cos(\varphi_m)$	$\frac{Ia_m}{4\pi\epsilon}G(y_{nm},x_{nm})$
$\sin(\varphi_m)$	$-\frac{a_m}{4\pi\epsilon}\ln\left(\frac{((y_{nm}+b_l)^2+x_{nm}^2)}{((y_{nm}-b_l)^2+x_{nm}^2)}\right)$
$\cos(j\varphi_m)$ $j\geq 2$	$-\frac{I^j a_m^j}{4j\pi\epsilon}\begin{pmatrix}T_1(y_{nm},x_{nm},j-1)\\+(-1)^jT_2(y_{nm},x_{nm},j-1)\end{pmatrix}$
$\sin(j\varphi_m)$ $j\geq 2$	$-\frac{I^{j+1} a_m^j}{4j\pi\epsilon}\begin{pmatrix}-T_1(y_{nm},x_{nm},j-1)\\+(-1)^jT_2(y_{nm},x_{nm},j-1)\end{pmatrix}$

$$G(\alpha,\beta)=H(\alpha,\beta,b_l)-H(\alpha,\beta,-b_l)$$

$$H(\alpha,\beta,\gamma)=\ln\left(\frac{-\alpha-\gamma+I\beta}{\alpha+\gamma+I\beta}\right)$$

$$T_1(\alpha,\beta,\gamma)=\frac{1}{\gamma}\left(\frac{(-1)^{\gamma+1}}{(b_l+\alpha+I\beta)^\gamma}+\frac{1}{(b_l-\alpha-I\beta)^\gamma}\right)$$

$$T_2(\alpha,\beta,\gamma)=\frac{1}{\gamma}\left(\frac{(-1)^{\gamma+1}}{(b_l+\alpha-I\beta)^\gamma}+\frac{1}{(b_l-\alpha+I\beta)^\gamma}\right)$$

$$\mathcal{G}(\alpha,\beta)=\begin{matrix}\mathcal{H}(\alpha+b_l+I\beta)+\mathcal{H}(\alpha+b_l-I\beta)\\-\mathcal{H}(\alpha-b_l+I\beta)-\mathcal{H}(\alpha-b_l-I\beta)\end{matrix}$$

$$\mathcal{H}(\alpha)=\alpha\ln(\alpha) \tag{36}$$

The submatrix in $\mathbf{M}_{l\to l}$ represents the contribution from the charges on line elements to the potentials on line elements. Since the potentials on the line elements only have a constant basis function, the formulas are the same as the formulas for constant basis function in (A).

B Approximate Equation for Adjacent Wires

The approximate equation for adjacent wires can be obtained from the proposed method. It has the form in (29), where the $F(N)$ is an order-related rational function. The function $F(2)$ is given in (37).

$$F(2)=\frac{\begin{matrix}(33\epsilon_{ins}^2+6\epsilon_{ins}-39)R_{ba}^6\\+(33\epsilon_{ins}^2+56\epsilon_{ins}+39)R_{ba}^4\\+(33\epsilon_{ins}^2-56\epsilon_{ins}+39)R_{ba}^2\\+(33\epsilon_{ins}^2-6\epsilon_{ins}-39)\end{matrix}}{2\begin{pmatrix}(37\epsilon_{ins}^2+126\epsilon_{ins}+93)R_{ba}^6\\+(37\epsilon_{ins}^2-8\epsilon_{ins}-93)R_{ba}^4\\+(37\epsilon_{ins}^2+8\epsilon_{ins}-93)R_{ba}^2\\+37\epsilon_{ins}^2-126\epsilon_{ins}+93\end{pmatrix}} \tag{37}$$

The function $F(4)$ is more complex and hard to fit on the page. Therefore, an asymptotic function is obtained from the $F(4)$ and is given in (38).

$$F(4)\approx\frac{\begin{matrix}2464287\epsilon_{ins}^4+7175412\epsilon_{ins}^3\\+2362986\epsilon_{ins}^2-7175212\epsilon_{ins}-4827473\end{matrix}}{\begin{matrix}4575852\epsilon_{ins}^4+31985424\epsilon_{ins}^3\\+73092168\epsilon_{ins}^2+68677776\epsilon_{ins}+22995372\end{matrix}}+\frac{256\epsilon_{ins}\begin{pmatrix}40287\epsilon_{ins}^3+169635\epsilon_{ins}^2\\+221853\epsilon_{ins}+92513\end{pmatrix}^2}{\begin{pmatrix}381321\epsilon_{ins}^4+2665452\epsilon_{ins}^3\\+6091014\epsilon_{ins}^2+5723148\epsilon_{ins}+1916281\end{pmatrix}^2}R_{ba}^2 \tag{38}$$

REFERENCES

[1] M. -V. Juan A., *Power System Transients: Parameter Determination*, J. A. Martinez-Velasco Ed., Boca Raton, FL, USA: CRC Press, 2017. [Online]. Available: https://www.taylorfrancis.com/books/9781420065305

[2] M. Popov, L. van der Sluis, R. P. P. Smeets, and J. Lopez Roldan, "Analysis of very fast transients in layer-type transformer windings," *IEEE Trans. Power Del.*, vol. 22, no. 1, pp. 238–247, Jan. 2007. [Online]. Available: https://ieeexplore.ieee.org/document/4039465/

[3] M. A. Saket, N. Shafiei, and M. Ordonez, "LLC converters with planar transformers: Issues and mitigation," *IEEE Trans. Power Electron.*, vol. 32, no. 6, pp. 4524–4542, Jun. 2017.

[4] B. Gustavsen, A. P. Brede, and J. O. Tande, "Multivariate analysis of transformer resonant overvoltages in power stations," *IEEE Trans. Power Del.*, vol. 26, no. 4, pp. 2563–2572, Oct. 2011.

[5] R. Aghmasheh, V. Rashtchi, and E. Rahimpour, "Gray box modeling of power transformer windings for transient studies," *IEEE Trans. Power Del.*, vol. 32, no. 5, pp. 2350–2359, Oct. 2017.

[6] F. Nasirpour, T. Luo, M. G. Niasar, and M. Popov, "Multi-winding power transformer modeling for fast-front transients," *IEEE Trans. Power Del.*, vol. 40, no. 2, pp. 1054–1066, 2025.

[7] A. Rezaei-Zare, "Equivalent winding capacitance network for transformer transient analysis based on standard test data," *IEEE Trans. Power Del.*, vol. 32, no. 4, pp. 1899–1906, Aug. 2017.

[8] Z. Shen, H. Wang, Y. Shen, Z. Qin, and F. Blaabjerg, "An improved stray capacitance model for inductors," *IEEE Trans. Power Electron.*, vol. 34, no. 11, pp. 11153–11170, Nov. 2019. [Online]. Available: https://ieeexplore.ieee.org/document/8672508/

[9] J. Biela and J. W. Kolar, "Using transformer parasitics for resonant converters - A review of the calculation of the stray capacitance of transformers," in *Proc. Conf. Rec. - IAS Annu. Meeting IEEE Ind. Appl. Soc.*, 2005, pp. 1868–1875. [Online]. Available: https://ieeexplore.ieee.org/document/1518701/

[10] A. Massarini and M. Kazimierczuk, "Self-capacitance of inductors," *IEEE Trans. Power Electron.*, vol. 12, no. 4, pp. 671–676, Jul. 1997. [Online]. Available: https://ieeexplore.ieee.org/document/602562/

[11] L. Dalessandro, F. da Silveira Cavalcante, and J. W. Kolar, "Self-capacitance of high-voltage transformers," *IEEE Trans. Power Electron.*, vol. 22, no. 5, pp. 2081–2092, Sep. 2007. [Online]. Available: https://ieeexplore.ieee.org/document/4300868/

[12] X. Liu, Y. Wang, J. Zhu, Y. Guo, G. Lei, and C. Liu, "Calculation of capacitance in high-frequency transformer windings," *IEEE Trans. Magn.*, vol. 52, no. 7, Jul. 2016, Art. no. 2003204.

[13] N. B. Chagas and T. B. Marchesan, "Analytical calculation of static capacitance for high-frequency inductors and transformers," *IEEE Trans. Power Electron.*, vol. 34, no. 2, pp. 1672–1682, Feb. 2019.
[14] H. Zhao et al., "Physics-based modeling of parasitic capacitance in medium-voltage filter inductors," *IEEE Trans. Power Electron.*, vol. 36, no. 1, pp. 829–843, Jan. 2021. [Online]. Available: https://ieeexplore.ieee.org/document/9119860/
[15] Q. Yu and T. Holmes, "A study on stray capacitance modeling of inductors by using the finite element method," *IEEE Trans. Electromagn. Compat.*, vol. 43, no. 1, pp. 88–93, Feb. 2001. [Online]. Available: https://ieeexplore.ieee.org/document/917948/
[16] Y. Tanaka and Y. Baba, "Development of a method for calculating the capacitance of cables installed in a rectangular tunnel taking account of the permittivity of the outer sheath," *IEEE Trans. Electromagn. Compat.*, vol. 65, no. 5, pp. 1422–1431, Oct. 2023.
[17] H. Nishiyama and M. Nakamura, "Form and capacitance of parallel-plate capacitors," *IEEE Trans. Components, Packaging, Manuf. Technol.: Part A*, vol. 17, no. 3, pp. 477–484, Sep. 1994. [Online]. Available: https://ieeexplore.ieee.org/document/311759/
[18] N. Malik, "A review of the charge simulation method and its applications," *IEEE Trans. Elect. Insul.*, vol. 24, no. 1, pp. 3–20, Feb. 1989. [Online]. Available: https://ieeexplore.ieee.org/document/19861/
[19] M. Naghed and I. Wolff, "Equivalent capacitances of coplanar waveguide discontinuities and interdigitated capacitors using a three-dimensional finite difference method," *IEEE Trans. Microw. Theory Techn.*, vol. 38, no. 12, pp. 1808–1815, Dec. 1990. [Online]. Available: https://ieeexplore.ieee.org/document/64560/
[20] J. Savage and W. Smith, "Capacitance calculations for cable harnesses using the method of moments," *IEEE Trans. Electromagn. Compat.*, vol. 37, no. 1, pp. 131–137, Feb. 1995. [Online]. Available: https://ieeexplore.ieee.org/document/350254/
[21] T. Luo, "Multicon2d_c," 2023. [Online]. Available: https://github.com/TMLuo/MultiCon2D_C
[22] J. Clements, C. Paul, and A. Adams, "Computation of the capacitance matrix for systems of dielectric-coated cylindrical conductors," *IEEE Trans. Electromagn. Compat.*, vol. EMC-17, no. 4, pp. 238–248, Nov. 1975. [Online]. Available: https://ieeexplore.ieee.org/document/4090922/
[23] T. Luo, M. G. Niasar, and P. Vaessen, "Two-dimensional frequency-dependent resistance and inductance calculation method for magnetic components with round conductors," *IEEE Trans. Magn.*, vol. 60, no. 1, Jan. 2024, Art. no. 8400211.
[24] P. Hammond, "Electric and magnetic images," *Proc. IEE Part C: Monographs*, vol. 107, no. 12, pp. 306–313, 1960. [Online]. Available: https://digital-library.theiet.org/content/journals/10.1049/pi-c.1960.0047
[25] M. Kazimierczuk, *High-frequency magnetic components*. Hoboken, NJ, USA: Wiley, 2013. [Online]. Available: https://onlinelibrary.wiley.com/doi/book/10.1002/9781118717806

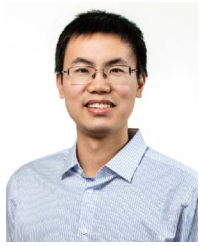

Tianming Luo (Member, IEEE) was born in Jinan, China in 1993. He received B.E. degree in electrical engineering and automation from Chongqing University, Chongqing, China, the M.Sc. degree from China Electric Power Research Institute and the Ph.D. degree from the Delft University of Technology, Delft, The Netherlands. He is currently a Postdoc Researcher with the Technique University of Denmark, Denmark. His research interests include multiphysic models of medium-frequency transformers, multi-objective optimization, and insulation performance under medium frequencies.

Mohamad Ghaffarian Niasar (Member, IEEE) was born in Tehran, Iran in 1984. He received the M.Sc. degree from the Sharif University of Technology, Tehran, Iran in 2008, and the Ph.D. degree in electrical engineering from the Royal Institute of Technology (KTH) in Stockholm, Sweden, 2015. He is currently an Associate Professor with the High Voltage Technologies Group, Delft University of Technology in Delft, The Netherlands. His main research interests include aging of insulation material, HVDC insulation system, high frequency power transformers, and multiphysics modeling of power components.

Peter Vaessen (Member, IEEE) was born in Maasbree, The Netherlands in 1960. He received the cum laude M.Sc. degree in electrical power engineering from Eindhoven Technical University, Eindhoven, The Netherlands in 1985, he joined KEMA (now a CESI brand). In his 35-year career he held research positions in the field of large power transformers and high voltage measurement and testing. He has 25 years of experience in (U)HVDC technology and T&D grids with high shares of renewables. He is currently a Manager innovations with KEMA Laboratories and the Chairman of the European Distributed Energy Resources Laboratories association (DERlab), and a Member of several national and international working groups. Since 2017, he has been a part-time Professor Hybrid Transmission Systems with TU Delft where he teaches high voltage technology and HVDC.